DIAGNOSTIC IMAGING

Radiology is divided into diagnostic radiology, interventional radiology, and radiotherapy. Diagnostic radiology encompasses not only X-ray imaging but all modes of noninvasive human imaging, which are listed in Table 1. Of these, the principal methods used since 1970 are planar X-ray methods (e.g., fluoroscopy, angiography, gastrointestinal contrast series, urography, myelography), X-ray computed tomography (CT), ultrasound (US), techniques of positron emission tomography [positron emission tomography (PET) and single photon emission computed tomography (SPECT)], nuclear magnetic resonance methods of magnetic resonance imaging (MRI), magnetic resonance angiography (MRA), and magnetic resonance spectroscopy (MRS) also known as chemical shift imaging. Currently 70% of all the conventional radiological procedures use X rays. About 60% of the initial diagnostic procedures are X-ray based with only 8% nuclear medicine emission, 3% ultrasound, and 3% MRI. Advances in imaging speed, resolution, and data processing are rapidly changing the relative importance of these modalities particularly in areas such as MRI, fast X-ray CT, ultrasound, and emission tomography. These main methods are described in general terms below with more technical details presented in (1,2) and elsewhere in this encyclopedia. Following a description of these methods, major medical applications are highlighted for all of the major organ systems along with selected radiologic images (Fig. 1).

X RAY

Presently the most widely used imaging modality is the X-ray transmission intensity projection, most commonly known as "the X ray." The difference between the X ray, a simple 2-dimensional projection image, and the X-ray computed tomograph, "the CT," is that the latter is the result of mathemati-

Table 1. Diagnostic Imaging Methods Summary

Method	Information
(1) X-ray (contrast, X-ray CT, electron beam CT, spiral CT)	Electron density Atomic composition Vascular lumens
(2) Ultrasound (US) Doppler Ultrasound	Acoustic impedance mismatches, Motion
(3) Emission Tomography (PET, SPECT)	Radionuclide concentration (metabolism, receptor densities)
(4) Magnetic Resonance Imaging (MRI), Spectroscopy (MRS), Angiography (MRA)	Spin density, relaxation, diffusion, Chemical composition
(5) Electrical Source Imaging (ESI)	Brain and heart current sources
(6) Magnetic Source Imaging (MSI); Magnetoencephalography[a] (MEG)	Brain current sources
(7) Electrical Impedance Tomography (EIT)	Electrical conductivity
(8) Optical Imaging (Spectroscopy)	Attenuation, scattering, molecular status

[a] Same as ESI.

J. Webster (ed.), *Wiley Encyclopedia of Electrical and Electronics Engineering*. Copyright © 1999 John Wiley & Sons, Inc.

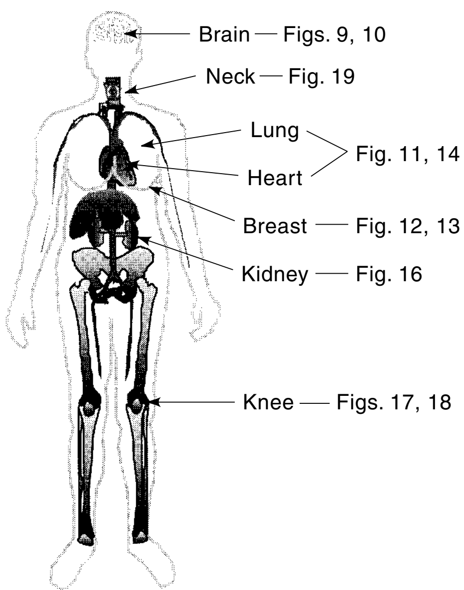

Figure 1. This, a guide to the second half of this article, gives selected imaging results to demonstrate applications of the major diagnostic methods.

cally reconstructing an image of a slice through the body from multiple X-ray transmission projection images taken at multiple angles (usually equal) around the body.

X rays are generated by the interaction of accelerated electrons with a target material such as tungsten. The electrons are produced by a heated cathode and accelerated by applying a voltage of about 100 keV between the cathode and a tungsten or molybdenum anode contained in a vacuum container called the X-ray tube or X-ray gun. The electron beam colliding with the anode releases X rays characteristic of the target materials. K-shell X rays from tungsten are about 70 keV and these as well as other X rays or photons are emitted from the X-ray tube placed one or more meters from the patient. The X-ray radiograph is usually a film, not unlike a photographic negative, which is darkened due to the interaction of the photons with the silver halide granules of the film. To enhance efficiency, a screen containing a phosphor is juxtaposed with the film. The electrons which interact with the phosphor release thousands of photons in the visible wavelength. The image reflects the number or intensity of photons reaching the film, and as is the case for a conventional negative, the greater the intensity, the darker the X ray. The intensity of photons transmitted through the body is modulated by the processes of Compton scattering and photoelectric absorption in tissue which are dependent on electron density and tissue elemental composition, respectively. These modulation processes are lumped into a simple attenuation coefficient. The intensity (or number) of photons arriving at a particular position, (x, y), on the X-ray film is given as

$$I(x, y) = I_0 e^{-\mu z} \tag{1}$$

where $I(x, y)$ is the photon intensity at position (x, y), I_0 is the intensity from the X-ray tube, μ is the attenuation coefficient (units of length^{-1}), and z is the path length through the patient to the image position x, y. This equation applies to a situation of constant attenuation along z. The attenuation coefficient of lung, water, tissue, and bone differ. Thus the intensity arriving at the film is more generally

$$I(x, y) = I_0 e^{-\sum \mu(x,y,z)\Delta z_i} \tag{2}$$

where we divided the path z into intervals Δz_i. Here we assume parallel X-ray paths and no magnification; otherwise the image coordinates would be different from the object coordinates. The contrast or intensity difference between a lung tumor region and the surrounding normal tissue, as recorded on a conventional projection X ray, is related to the difference in number of photons projected through the tumor and through the parallel paths surrounding the tumor. This difference in number of photons would be about 23% for a 3-cm tumor, but the contrast visualized will depend on the image detector (e.g., silver halide film, solid state detector).

Recall the fact that as the number of photons decreases the less the exposure of the X-ray film and the "whiter" the image in that region. X-ray imaging is mainly an anatomical procedure. The absorption of X rays due to differences in elemental composition has an important effect for imaging bone or calcium deposits because this absorption process is proportional to the atomic number. To provide image contrast between the blood vasculature and surrounding tissue, a dense fluid with elements of high atomic number (e.g., iodine, barium) can be injected or swallowed during the X-ray exposures. The movement through the body vasculature of a "contrast agent" such as an iodinated compound can be visualized by acquiring a sequence of X rays. The iodine or barium agent absorbs photons more than blood and tissue because the density is higher and the elements iodine and barium have a high atomic number giving rise to more photoelectric absorption.

X-RAY CT

X-ray transmission computed tomography (X-ray CT) gives anatomical information of the tissues mainly based on the density and elemental composition in specific regions as derived by manipulation of the projections of X rays through the body at multiple angles. It is useful to examine the log of the ratio of incoming intensity to the exiting intensity to parameterize these projections

$$P(x, y) = \ln \frac{I_0}{I(x, y)} = \sum_{i \in \text{ray}\, x, y} \mu(x, y, z_i)\Delta z_i \tag{3}$$

Note the logarithm of the intensity ratio which we designate a projection $P(x, y)$ is simply the line integral of attenuation coefficients along the path orthogonal to x, y if the Δz_i's approach zero. Thus for each angle:

$$P_{(x,y)} = \int_{\text{Source}}^{\text{Detector}} \mu(x, y, z)\, dz \tag{4}$$

This summation is called a ray sum and the projection position is called a bin. The usefulness of this manipulation is that we can work with projections in a linear fashion to reconstruct the 3-dimensional distribution of linear attenuation coefficients and thus create an X-ray computed tomograph using linear operations discussed below. The denser the

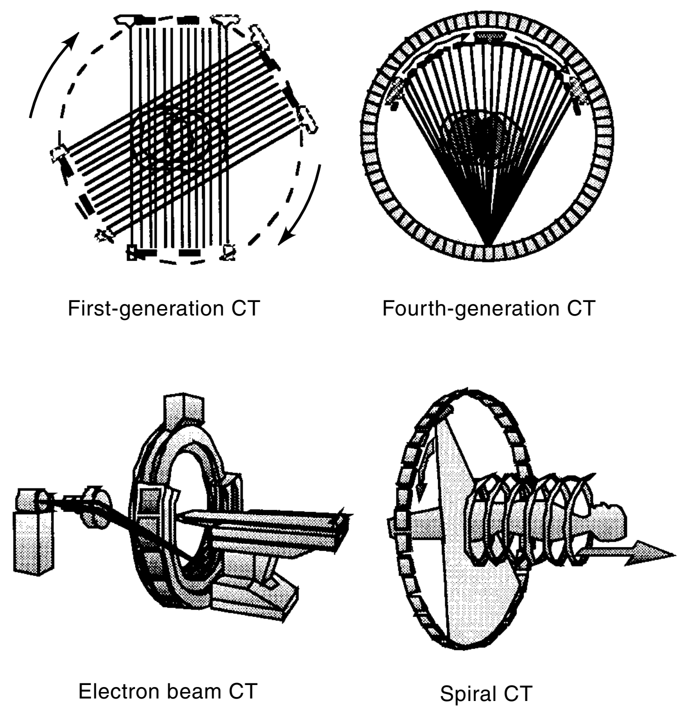

Figure 2. X-ray computed tomography has evolved to rapid scanning systems over the last 25 years. Electron beam techniques can scan a few transverse sections without distortion from heart motion, and spiral X-ray CT can cover the abdomen with 2 breath-holds at 1 s per each transverse section.

electrons, the more the X-ray beams are scattered or attenuated. In addition, the absorption of X rays due to the photoelectric effect has important effects. Indeed the reason there are small differences between gray from white matter in the brain in CT images is that the H, C, N, O, P content for gray and white matter differ slightly resulting in about 3% changes between gray and white matter.

The 3-D reconstruction in X-ray CT is the composite of a stack of 2-D transverse planes. A single 2-D transverse plane or tomograph consists of pixels whose values are proportional to the attenuation coefficients (i.e., scattering from electron density and photoelectric absorption). Individual solid state detectors are used for X-ray CT wherein the photon intensity is recorded as current generated in the detector for a given time interval. To perform the reconstruction, many one-dimensional projections are acquired from multiple angles. The idea is shown as the “1st generation CT” in Fig. 2. From these multiple projections the map or image of the anatomy in a particular slice is mathematically reconstructed using a computer, thus the word CAT for *computer assisted tomography*. The main method of reconstruction involves Fourier transformation of each projection, application of a ramp filter, inverse Fourier transformation, and back projection. This process is equivalent to back projection of each projection after each has been convolved with a kernel which is the Fourier transform of a ramp in spatial frequency space, thus the terminology “convolution method” (3). The contemporary trend for X-ray CT is to acquire finer resolution at high speed. These innovations have application to moving organs wherein data can be collected during 10 s to 16 s of breath holding.

In spiral CT slip-ring technology provides continuous 360° rotation of the X-ray gantry for up to 40 s (4). Because the table continuously moves the patient through the gantry during scanning, the projection data are collected along a continuous spiral path instead of as parallel transaxial slices in conventional X-ray CT. The simultaneous table movement and continuous gantry rotation (gantry rotation period is 1 s) without an interscan delay allow data to be collected very rapidly. When using intravenously administered iodinated contrast, images of the abdomen can be captured when the contrast is in the arterial or venous phase of the circulation. A typical high resolution ($\leq$3 mm collimation) spiral examination of the abdominal aorta can be performed in 30 s covering 9 to 18 cm of volume. A conventional CT scan may take several minutes to cover the same column and therefore cannot precisely image during the arterial contrast phase. This mode has brought X-ray CT applications to lung and abdominal scanning including data acquisition for virtual bronchoscopy and virtual colonoscopy.

Electron Beam Computed Tomography (EBCT)

Another mode of fast X-ray scanning with or without contrast injection employs an accelerated electron beam that strikes an anode target consisting of a large arc of tungsten encircling about 225 degrees transaxial to the patient (Fig. 2). The purpose is to avoid motion blurring from heart motion and to achieve an image sampling fidelity sufficient to evaluate the flow of contrast through the vascular and extracellular spaces mainly for heart, lung, aorta, kidney, and sometimes brain studies. EBCT applications are mainly for evaluation of coronary calcium and usually involve acquisition of 40 contiguous 3-mm thick sections extending from the right pulmonary artery to the heart apex. Each section is timed for acquisition during late diastole using ECG triggering and breath holding to minimize heart motion effects.

Digital X-Ray Systems and Digital Radiology

Though the present standard detector is X-ray film wherein the efficiency is enhanced by a phosphor which converts X rays to light photons for subsequent film exposure, there is a major technological development to deploy flat-panel imaging systems using solid-state detectors for direct electronic readout to supplant the screen-film based systems. This is part of the conversion of diagnostic imaging centers to an all digital electronic-based imaging and information communication center. All of the radiological imaging methods with the exception of the most commonly used X ray are digitally based. It is estimated that approximately 70,000 radiographic units in the United States will be retrofitted by digital detectors in the next few years. The present number of mammography units in the United States is approximately 11,000 and there is currently a major effort to create a digital system capable of providing a resolution at least as good as 50 μm (10 line pairs per mm) which is one-half as good as the contemporary screen film analog mammography systems. The benefits anticipated for digital mammography systems are great if the systems can meet the design criteria including resolution, image acquisition time, and heat loading of the X-ray tube (5). The technologies now being evaluated range from miniature 200 μm or less pixel-based, direct X-ray electronic detectors.

A proposed mode uses complementary metal oxide semiconductor (CMOS) electronics coated with selenium for real-time readout of electrons generated by the X rays striking the detector. Another mode uses cesium iodide scintillators coupled to silicon photodiodes or amorphous silicon solid state two-dimensional arrays to allow direct electronic readout into computer systems. These are developments which go beyond the charged coupled devices (CCDs) which have been limited to wafers (12-cm diameter) which are too small for general radiographic replacement without elaborate methods to expand the field of view using optical systems and multiple wafers.

A new concept in X-ray imaging embodied in the digital detector is known as reverse geometry imaging which matches a large X-ray source to a small solid state detector. The X rays are created using an electron beam which scans a 2-dimensional anode through magnetic deflection. A cone of X rays are focused onto a small solid state detector which records the attenuation through each patient position. The ideal detector for this application is cadmium zinc telluride (CZT) which is too expensive to make into panels for large field of view digital radiography. The concept of reverse geometry overcomes the size limitations and though designed for fluoroscopy, this innovation has other applications including breast mammography. Digital radiology systems facilitate image enhancement, calibration, distortion removal, and communications including storage, dissemination, consultation, and teleradiology.

ULTRASOUND

Ultrasound, as currently practiced in medicine, is a real-time tomographic imaging modality. Not only does it produce real-time tomograms of the position of reflecting surfaces (internal organs and structures), but it can be used to produce real-time images of tissue and blood motion due to the Doppler effect.

Ultrasound uses longitudinal compression waves generated by the voltage-induced oscillations of a piezoelectric crystal which is typically a ceramic disk consisting of lead zirconium titinate (PZT). The oscillations are at frequencies of 0.5 MHz to 20 MHz. The ultrasound is a coherent pressure wave which is reflected from surfaces of varying acoustic impedances, Z (Z = tissue density $\times$ velocity of sound in tissue). Loss of ultrasound energy dissipated as heat is at about 2 dB per cm for 2 MHz. This dissipation is due to loss of coherence. The ultrasound scatters from surfaces and this scattering is proportional to frequency. The attenuation amounts to 1 dB per cm tissue depth for each MHz. Thus at 3 MHz the loss at 2 cm of tissue penetration is 6 dB or a halving of the signal strength. Thus for imaging the heart in children 5 MHz can be used but for imaging an adult abdomen frequencies are usually 1 MHz.

The major uses of ultrasound are in the examination of the carotid arteries, heart value function, heart wall motion, gall bladder, and examination of the pregnant abdomen including the anatomy of the fetus.

The technique is to sonicate tissues with a transducer coupled by Vaseline to the skin surface over the area of study (e.g., carotid arteries, heart, gall bladder, uterus in pregnant women). The location of surfaces within tissues is determined

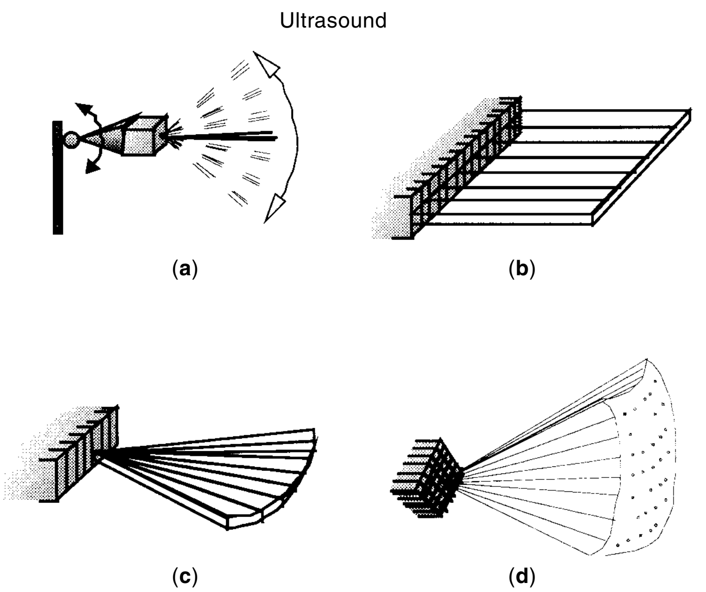

Figure 3. Modes of ultrasound imaging which allow direct 2-D evaluation by mechanical scanning (a) or electronic scanning at frequencies between 1 to 5 MHz (b–d). Catheter-tip transducers are also available for vascular wall studies using 10 to 20 MHz frequencies.

by measuring the time interval between the production of an ultrasonic pulse and the detection of its echo resulting from the pulse reflected from those surfaces. By measuring the time interval between the transmitted and detected pulse, we can calculate the distance between the transmitter and the object.

$$d = \frac{1}{2} t \cdot c \tag{5}$$

where c is the speed of sound in tissue, ca. 1450 $\mathrm{m \cdot s^{-1}}$. The ultrasound pulses are both produced and detected by the piezoelectric crystal or transducer. The reflected ultrasound imposes a distortion on the crystal, which in turn produces an oscillating voltage in the crystal. The same crystal is used for both transmission and reception. Types of ultrasound instruments are shown in Fig. 3. In addition to imaging (discussed under organs below), ultrasound is being used for monitoring therapy methods such as hyperthermia, cryosurgery, drug injections, and as a guide during biopsies and catheter placements. Tissue acoustic impedance changes with temperature, the material being injected, and the metal or plastic surfaces of the catheters.

Doppler Ultrasound

If a structure is stationary, the frequency of the reflected wave will be identical to that of the impinging wave. A moving structure will cause a backscattered signal to be frequency shifted higher or lower ($\pm\Delta f$) depending on the structure's velocity toward or away from the sound generator or transducer. The Doppler equation is

$$\Delta f = \frac{-2f_0 v \cos\theta}{c + v} \approx \frac{-f_0 v \cos\theta}{c} \tag{6}$$

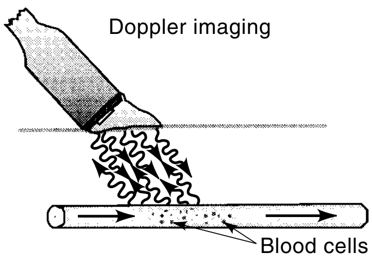

Figure 4. A major use of ultrasound is evaluation of blood flow in particular in the carotid arteries of the neck. The frequency changes associated with moving blood cells can give speed and direction of moving blood cells toward or away from the transducer.

where f_0 is the transmission frequency, (v) is the velocity of the moving cells, (c) the velocity of sound, and θ the angle between the transducer axis and the flow axis.

For example, when an impinging sound pulse passes through a blood vessel, scattering and reflection occurs from the moving red cells (Fig. 4). In this process, small amounts of sound energy are absorbed by each red cell, then reradiated in all directions. If the cell is moving with respect to the source, the backscattered energy returning to the source will be shifted in frequency, with the magnitude and direction proportional to the velocity of the respective blood cell. Thus, if we use ultrasound to image the cross-sectional area of the blood vessel, the volume of blood flow can be calculated from the area of the vessel and the average velocities of the blood cells. The frequency shift data are color coded (e.g., carotid arteries in red and veins in blue) to form 2-D images. Image positional data are provided by the range (distance) of the signal whose frequency shift gives the speed at that range. Obstructions to blood flow are readily evaluated by this method using hand-held scanning devices.

Power Doppler is a relatively new method of imaging the partial volume of moving blood. The sum of the square power of all frequency shifts gives information about the number of moving surfaces independent of direction. A local increase in vascularity as seen in breast cancer and lymph node metastases will give a relatively high power doppler signal.

MAGNETIC RESONANCE IMAGING

Magnetic resonance imaging (MRI) has evolved into one of the most powerful noninvasive techniques in diagnostic imaging and biomedical research. MRI uses the principles of a well-known analytical method of chemistry, physics, and molecular structural biology. However, this basic method has been slightly modified by applying relatively small spatial magnetic field gradients of varying amplitudes and directions to achieve spatial information of the density and characteristics of nuclei with magnetic spins. MRI is primarily used as a technique for producing anatomical images, but as described below, MRI also gives information on the physical–chemical state of tissues, flow, diffusion, and motion information. Magnetic resonance spectroscopy (MRS) gives chemical composition information.

Most elements have at least one reasonably abundant isotope whose nucleus is magnetic. In biological materials, the magnetic nuclei of ^{1}H, ^{13}C, ^{23}Na, ^{31}P, and ^{39}K are all abundant. The hydrogen nucleus (a single proton) is abundant in the body due to the high water content of nonbony tissues. When the body is immersed in a static magnetic field, slightly more protons become aligned with the magnetic field than against the static field (Fig. 5). At 1 T (10,000 gauss) and 25 °C the difference between these aligned populations of about one proton in a million produces a net magnetization. The net magnetization precesses around the static field at a frequency,

$$\omega = 2\pi v = \gamma B \tag{7}$$

where ω is frequency, γ is the gyromagnetic ratio particular to each nuclear species, and B is the field.

A rapidly alternating magnetic field at the resonant frequency ω, applied by a coil near the subject or specimen in the static magnetic field, changes the orientation of the net magnetization relative to the direction of the static magnetic field.

These changes are accompanied by the absorption of energy (from the alternating magnetic field) by nuclei which undergo the transition between energy states. When the alternating field is turned off, the nuclei return to the equilibrium state, emitting energy at the same frequency as was previously absorbed. The nuclei of different elements, and even of different isotopes of the same element, have very different resonance frequencies. For a field of 1 T (10,000 gauss), the resonance frequency of protons is 42 MHz and that of phosphorus is 17 MHz. Thus, the magnetic nuclei in the body, when placed in a static magnetic field, can be thought of as tuned receivers and transmitters of RF energy. The governing relation is Eq. (7). Unlike its X-ray counterparts, MRI is not a transmission technique. Rather, similar to PET and SPECT, the material imaged is in itself the signal source (i.e., the polarized nuclear spins).

The motion of the macroscopic nuclear spin magnetization, **M** is conveniently described in terms of the phenomenological Bloch equation:

$$\frac{d\mathbf{M}}{dt} = \gamma \mathbf{M} \times \mathbf{B} - \frac{M_{xy}}{T_2} - \frac{M_z - M_0}{T_1} \tag{8}$$

where M_0 is the equilibrium magnetization, and T_1 and T_2 are relaxation times. T_1 is the characteristic relaxation time for longitudinal magnetization to align with the magnetic field: following a perturbation such as an RF pulse or a change in

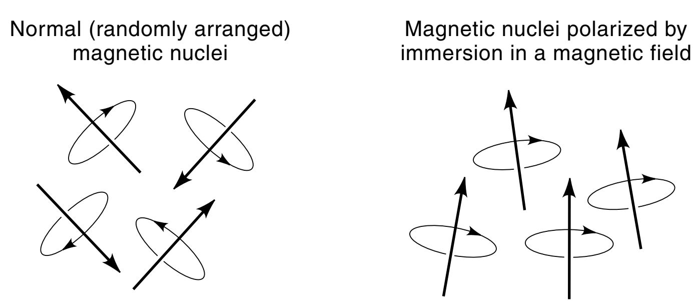

Figure 5. Magnetic resonance imaging is based on detection of the net magnetism of nuclei which have magnetic spin such as the hydrogen nuclei (protons) of tissue water. The detection is facilitated by RF pulses which stimulate signals from the oriented nuclei.

magnetic field, the longitudinal magnetization typically returns to its equilibrium value, M_0, with a time constant T_1. T_2 is the characteristic time for decay of coherent magnetization in the transverse plane: the transverse magnetization decays exponentially with time constant T_2 to its equilibrium value, $M_{xy} = 0$. For proton MRI, both relaxation times are determined by interaction of water with macromolecules in tissues. The dependence of image contrast on these parameters is appreciated by the equation components of the signal from a typical spin echo experiment:

$$S(t) = f(v)\rho(1 - \exp(-TR/T_1))\exp(-TE/T_2) \tag{9}$$

where $f(v)$ is a flow function, ρ is the density of ^{1}H (protons), TR the pulse sequence time interval, and TE the time to detect the echo from a 180° pulse applied TE/2 after the 90° RF pulse. Tissues have T_1 values which vary from 600 ms to 3000 ms (cerebral spinal fluid) and T_2 values of 20 ms to 40 ms, except tumors whose values can be greater than 60 ms. The time needed to acquire MR images was thought to be prohibitive for functional studies such as done with X-ray angiography; however, when it was discovered that flip angles less than 90° for the RF pulse could be used for MRI with acceptable signal to noise ratios and tissue contrast, a major horizon for contemporary studies was discovered (6). Now single slices can be obtained in less than 40 ms.

The principal components of the MRI machine are the magnet, radio frequency (RF) coils, and the gradient coils. The gradient coils are used to acquire spatial information. Note that if Eq. (7) is modified by superposing a spatial gradient $\Delta B/\Delta x$ on the large static field, there will be a frequency shift in accord with

$$\omega + \Delta\omega(x) = \gamma\left(B + \frac{\Delta B}{\Delta x}x\right) \tag{10}$$

It can be seen that the frequency for any nuclei at position x will be

$$\omega + \Delta\omega(x) \tag{11}$$

The received signal for all the nuclei in the space being imaged will be the linear superposition of the respective frequencies with amplitudes and individual signal decay characteristics (i.e., T_1 and T_2) determined by the local tissue biophysics at each spatial position. Three-dimensional information is gleaned by varying gradients in the x, y, z directions. The Fourier transform of this complex signal gives directly the image projections of intensities of nuclear magnetization. Reconstruction is implemented by back projection of these projections with appropriate filtering as is done in X-ray CT. An alternate reconstruction strategy involves use of phase alterations to encode information related to spatial positions of the nuclei. The RF coils used to excite the nuclei usually are quadrature coils which surround the head or body, but small (e.g., 6 to 10 cm) flat coils placed on the surface of the head or body are also used. Besides being the essential element for spatial encoding, the gradient-coil subsystem of the MRI scanner is responsible for the encoding of specialized contrast such as flow information, diffusion information, and modulation of magnetization for spatial tagging.

Magnet types in current use are of the superconducting, resistive, and permanent magnet designs ranging in strength

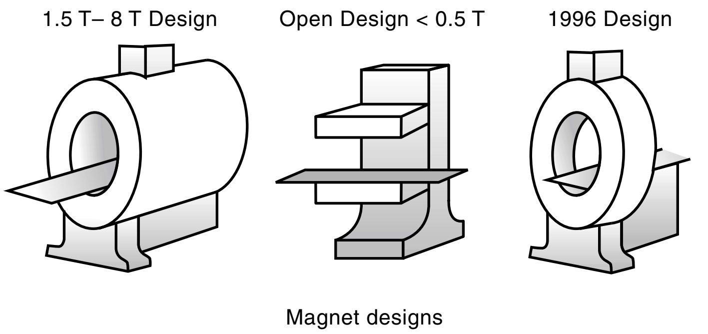

Figure 6. Magnets used for human imaging use superconducting wire in liquid helium systems or permanent magnet elements arranged around the subject for fields of about 0.3 T. Technological advances have allowed open designs for fields up to 1.5 T using superconductor wire.

from 0.06 to 4 T and have evolved from 2-m-long cylinders to more open designs for patient access and acceptability (Fig. 6). The majority of MR systems use superconducting magnets which provide fields of 1.5 T. Most currently produced magnets are based on niobium–titanium (NbTi) alloys, which are remarkably reliable, but require a liquid helium cryogenic system to keep the conductors at approximately 4.2 K (−268.8°C).

MRI Contrast Agents

MRI contrast agents are used to demonstrate perfusion and vasculature of organs. The usual contrast agents are water-soluble chelates of gadolinium. The chelates distribute in the vasculature and interstitial spaces much like the iodine contrast agents used for X-ray CT. Gadolinium causes an increase in the relaxation rates of the tissue water, thus, a decrease in T_1 and T_2. Presence of the gadolinium results in a signal enhancement on the images produced by pulse sequences which are designed to give higher signal for tissues with short T_1 [e.g., short TR in Eq. (9)]. Manganese complexed to a chelate accumulates intracellularly in some tissues and also causes T_1 shortening which leads to signal enhancement. Other types of contrast agents used by MRI are colloidal iron oxides (e.g., magnetite) coated with dextran which cause a MRI signal decrease in the region of their accumulation or a transient signal decrease as they perfuse through tissue due to the increase T_2 relaxivity [short T_2 times cf. Eq. (9)] of local tissue protons.

Magnetic Resonance Spectroscopy (MRS)

The nuclei constituting compounds in the human body have a resonance frequency governed by Eq. (7) relative to the imposed magnetic field. A nucleus of hydrogen will be in a slightly different magnetic field than the imposed magnetic field from the magnetic resonance magnet because adjacent spinning nuclei generate a small local field that shifts the frequency a few parts per million. Thus the protons of lactate are shifted in frequency by a few hundred hertz from the resonance frequency of water protons of 64 MHz at 1.5 T. This shift is known as the chemical shift and the resulting magnetic resonance spectrum gives specific information about the concentration of compounds in tissue noninvasively. Thus by manipulating the MRI gradients, selected regions can be sampled to determine the concentrations of tissue constituents containing hydrogen-1, carbon-13, phosphorus-31, and other NMR nuclei. As the spectra change with disease states, MRS has an important role in diagnoses of diseases, particularly brain cancer, prostate cancer, epilepsy, and brain trauma.

The sensitivity of MRS is very low, thus only tissue constituents with concentrations in the millimolar range are evaluated in selected volumes usually greater than 0.2 mL ($6 \times 6 \times 6$ mm) for proton spectroscopy and greater than 1 mL for phosphorus spectroscopy. The sensitivity increases with field strength and MRS imaging, though feasible for low-resolution imaging of protons for maps of choline-containing compounds, N-acetylaspartate, lactate, and lipids.

Functional Magnetic Resonance Imaging (fMRI)

Though 25 years ago nuclear medicine methods demonstrated flow changes associated with mental activity in humans, it was not until the less invasive (i.e., no radioactivity) methods of MRI showed a magnetic resonance signal associated with stimulation of the brain that the medical scientists embraced fMRI as a method for mapping brain function. Methods that reflect brain activity currently use the fact that in response to a stimulus (e.g., light flash, sound, touch, physical movement), there is an increase in local blood volume and blood flow in order to supply that region of the brain with oxygen and nutrients. The local blood flow in areas of 5 mm or more around the part of the brain being stimulated is in response to an increase in metabolism and electrical activity. Radioactive tracers have shown this functional response and MRI measurements can also show flow changes using injected contrast material such as Gd-EDTA or Gd-albumin or other methods of detecting flow (see above). However, the principal method now employed by fMRI relies on an intrinsic change in the local magnetic field associated with a change in the partial volume of oxygenated hemoglobin (diamagnetic) and deoxygenated hemoglobin (paramagnetic). The process is known as the BOLD (blood oxygen level dependent) effect.

The presence of paramagnetism from deoxyhemoglobin in capillaries, arterioles, and venules causes a magnetic field gradient across the imaging pixel sufficient to lower the MR signal. The positive BOLD signal is due to the effective decrease in paramagnetism and associated magnetic gradients over ranges less than 1 mm due to an increase in the partial volume of diamagnetism associated with more oxyhemoglobin in the region of activation. The fMRI is a map of the result of subtraction of the MRI before the activation from the MRI obtained by fast imaging methods performed during the activation. The more paramagnetism or deoxyhemoglobin the lower the signal and when one subtracts the MRI image taken before the activation from that taken after the activation the region of activation will appear relatively darker (a negative BOLD signal).

The almost universal findings from studies done at 1.5 T show a positive BOLD signal (e.g., a 2% change), and until recently, this was thought to represent an in-flow of diamagnetic oxyhemoglobin because the brain was not extracting metabolic oxygen; however, using fields of 4 T it has been shown that the positive BOLD signal is preceded by a negative BOLD signal which corresponds to an initial decrease in blood oxygen (more paramagnetism) within 0.5 s of the activation followed by an over-compensation of blood rich in oxygen to the activated region of the brain. Thus there is initially an increase in oxygen extraction, local blood volume possibly first of the capillary bed and then a compensatory increase in the regional flow of oxygenated blood leading to less local magnetic field distortion and thus a positive signal when the before activation image is subtracted from the activation image. The positive BOLD signal, though not precisely positioned at the area of activation due to the overflow phenomenon, is used in clinical medicine to aid in epilepsy and tumor surgery by showing the neurosurgeon which vital areas of the brain to avoid in the surgical procedure. Magnetoencephalography is also used for this purpose and the combination of fMRI and MEG can give improved functional brain activity maps.

RADIONUCLIDE EMISSION IMAGING (NUCLEAR MEDICINE IMAGING)

Nuclear medicine imaging, also known by the terms emission imaging, radio-isotope imaging, scintigraphy (i.e., making pictures of the scintillations from crystals), is the technique of making images of the distribution of radioactive compounds. The two major elements of this method are the type of radiopharmaceutical which is injected into the patient and the type of scanner or camera (e.g., Anger camera, PET, SPECT) used for detection of gamma radiations from the radioactive isotope in the injected compound (Fig. 7). The particular diagnostic application relies on the fact that radiopharmaceuticals go to different organs in varying amounts depending on the disease state and the type of radiopharmaceutical. An example of this technique is the use of radioactive iodine to map the metabolic activity of the human thyroid gland in the neck. As about 25% of the ingested or injected iodine accumulates in the thyroid within 24 h as part of the process of making thyroid hormone, it is possible to detect trace amounts of radioactive iodine by use of nuclear detectors, and to make images of the thyroid. These are not anatomic images but are images reflecting the spatial distribution of metabolic activity.

The majority of contemporary nuclear medicine studies are for brain blood flow, heart flow with and without induced stress by exercise or a pharmacologic agent, bone tumor scanning, thyroid scanning, and cancer detection. Specialized studies such as the detection of internal bleeding by injection of the patient's red blood cells after labeling with Tc-99m and a host of other applications are enabled by use of specific tracers. The radiation dose to the patient is about equivalent to that from background radiation of one year (i.e., 0.1 cGy) with a maximum to any organ equivalent to a back X-ray examination (i.e., 1 cGy). Table 2 lists a few of the commonly used agents and their applications.

Positron Emission Tomography (PET)

Whereas most radioactive isotopes decay by release of a gamma ray and electrons, some decay by the release of a positron. A positron is similar to an electron but has a positive charge. PET imaging begins with the injection of a biological molecule that carries with it a positron-emitting isotope (for example, ^{11}C, ^{13}N, ^{15}O, or ^{18}F). Within minutes, the isotope accumulates in an area of the body for which the molecule has an affinity. As an example, glucose labeled with ^{11}C (half-life, 20 min), or a glucose analog labeled with ^{18}F (half-life, 1.8 h),

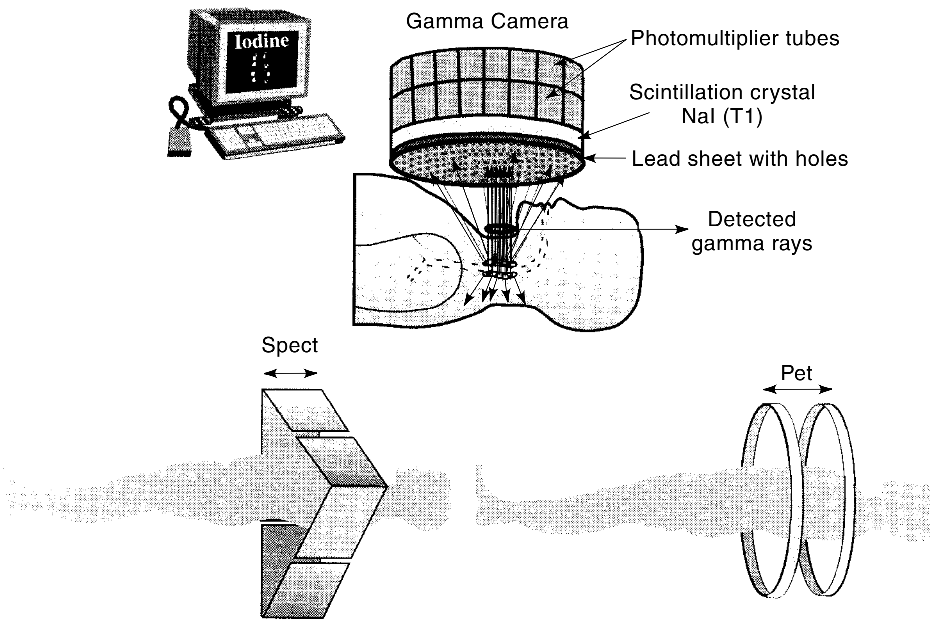

Figure 7. The three commonly used instruments for imaging radionuclides (nuclear medicine imaging). Relative sensitivity is determined by the area of detector material to which a source is exposed. For conventional gamma camera imaging the sensitivity is related to the solid angle ($d_1^2/4\pi r^2$) provided by the detector or proportional the resolution divided by the distance squared between the radiation and the detector. For PET the sensitivity is related to area (not resolution) of detector material divided by $4\pi r^2$.

accumulates in the brain, where glucose is used as the primary source of energy. The radioactive nuclei then decay by positron emission. The emitted positron collides with a free electron usually within 1 mm from the point of emission. The interaction of the two subatomic particles results in a conversion of matter to energy in the form of two gamma rays, each with an energy of 511 keV (note: $E = mc^2 = 511$ keV for the mass of each particle). These high-energy gamma rays emerge from the collision point in opposite directions ($180° \pm 0.25°$), and are detected by an array of detectors which surround the patient (Fig. 8).

When the two photons are recorded simultaneously by a pair of detectors, the nuclear decay that gave rise to them must have occurred somewhere along the line connecting the detectors. If one of the photons is scattered then the line of coincidence will be incorrect. After 500,000 or more annihilation events are detected, the distribution of the positron emitting tracer is calculated by tomographic reconstruction procedures. PET usually reconstructs a two-dimensional image. Three-dimensional reconstructions can also be done using 2-D projections from multiple angles (7).

The sensitivity of PET to detect nanomolar concentrations of tracers distinguishes this modality and its applications from those of MRI and MRS. MRI has exquisite resolution for anatomic studies and for flow or angiographic studies. In addition, magnetic resonance spectroscopy (MRS) has the unique attribute of evaluating chemical composition of tissue but in the millimolar range rather than the nanomolar range. Since the nanomolar range is the concentration range of most receptor proteins in the body, positron emission tomography is ideal for this type of imaging.

Table 2. Selected Radionuclides and Associated Imaging Targets

Radioactive Compound	Organ
^{123,131,122a}Iodine	Thyroid
Iodine compounds	Tumors
	Brain neuroreceptors
^{201}Tl, $^{13}NH_3^{a}$, $^{62}Cu^{a}$	Heart muscle
^{99m}Tc	
Pyrophosphate	Bone
DTPA	Kidney
HMPAO	Brain
Peptides	White blood cells and platelets
Sestamibi	Heart
Sulfur collide	Liver
^{111}In compounds	Tumors
^{67}Ga	Tumors
$^{18}F^{a}$	Bone
$^{18}F^{a}$ —deoxyglucose	Brain, heart, tumor
—neuroreceptor ligands	Brain neuroreceptors
$^{15}O^{a}$—H_2O	Brain blood flow
—O_2	Brain, heart, tumor

^{a} = positron emitters

Single-Photon Computed Tomography (SPECT)

SPECT, like PET, acquires information on the spatial distribution of radionuclides injected into the patient. As in X-ray CT, SPECT imaging involves the rotation of a photon detector array around the body to acquire data from multiple angles. Because the emission sources (injected radionuclides) are inside the body cavity, the reconstruction tomography task is far more difficult than for X-ray CT, where the source position and strength (outside the body) are known at all times. In X-ray CT the attenuation is measured, not the source strength. In PET and SPECT the reconstruction problem requires determination of the source position and strength (concentration) which is a much more difficult problem than simply determining the attenuation coefficient distribution. To compensate for the attenuation experienced by emitted photons from injected tracers in the body, contemporary SPECT machines use mathematical reconstruction algorithms more complex than those needed for X-ray CT (8).

SPECT sensitivity is inferior to PET thus the attainable resolution of SPECT is limited due to a statistical limitation

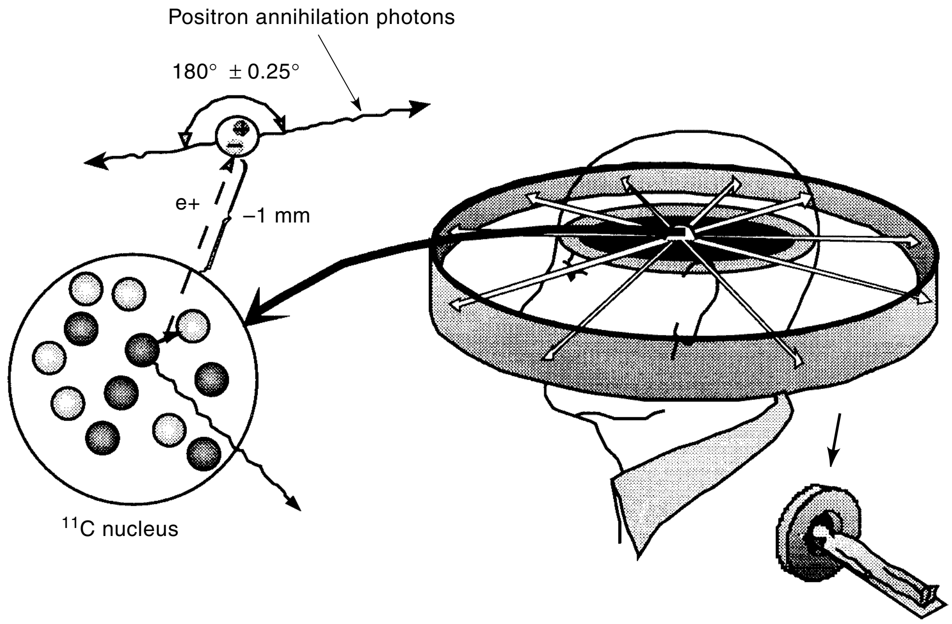

Figure 8. The PET isotopes usually have more protons than neutrons and when a proton becomes a neutron the positron (positive electron) is released which encounters an electron. Positron and electron pair masses annihilate creating two photons that disperse at 180° to be detected by PET sensors.

associated with acceptable amounts of injected radionuclides. Radionuclides used for SPECT imaging emit a single photon (e.g., 140 keV for ^{99m}Tc, 160 keV for ^{123}I) but the positron emitters (e.g., ^{11}C, ^{13}N, ^{15}O, ^{18}F) result in two 511 keV photons for PET detection. Because only a single photon is emitted from the radionuclides used for SPECT, a special lens known as a collimator is used to acquire the image data from multiple views around the body. The use of a collimator results in a significant decrease in detection efficiency as compared with PET. In PET, collimation is achieved naturally by the fact that a pair of detected photons (gamma rays) can be traced to a line after being produced. In PET, there might be as many as 500 detectors that could "see" a PET isotope at any one time where as in SPECT, there may be only 1, 2, or 3 collimators; thus, only 1, 2, or 3 detectors are available to each resolution volume in the subject. The statistics needed for reliable images and practical radioactive dose limitations limit the useful resolution of SPECT. The resulting useful resolution (about 7 mm) for SPECT is inferior to PET resolutions of about 4 mm for contemporary commercial systems and 2 mm for current research instruments.

Although SPECT imaging resolution is not that of PET, the ready availability of SPECT radiopharmaceuticals, particularly for the brain and head, and the practical and economic aspects of SPECT instrumentation make this mode of emission tomography attractive for clinical studies of the brain, heart, bone, and tumors (i.e., tumor metastases).

ENDOSCOPY

Endoscopy (i.e., visualization of the lumen of human conduits such as blood vessels and intestines) ranks among the most important advances in imaging over the last few decades. Unlike ultrasound, X-ray CT, and MRI, however, endoscopy has not in general been embraced by radiologists, being largely performed by other specialists and often viewed as competitive with well-established radiologic techniques.

The modern endoscope is a complex instrument requiring considerable precision in its construction. The shafts are circular in cross section with diameters dependent on the function of the instrument. Upper gastrointestinal instruments vary in diameter from 8 to 13 mm, side viewing duodenoscopes are 10 to 13 mm, and colonoscopes can be 15 mm in diameter.

There are two principal forms of the endoscope: the fiberoptic endoscope and the video endoscope. In the former the shaft carries a fiberoptic–optic bundle to transmit light, and a second fiberoptic–optic bundle (the viewing bundle) transmits an image to a lens system in the eyepiece of the endoscope. The fibers in this bundle retain their spatial relationship to each other throughout their length in order to transmit the image. Video endoscopes are now becoming the preferred type. The viewing bundle is replaced by a high-resolution video "chip" at the tip of the endoscope. The image is displayed on a color monitor which is more comfortable for the endoscopist, facilitates image storage and manipulation, and aids training by dynamic image access by multiple viewers. The shaft of both types of endoscopes accommodates a "working channel" (up to 4.2 mm in the largest side-viewing duodenoscopes) for the passage of accessories such as biopsy forceps, baskets, balloons, snares, and stents.

INTERVENTIONAL RADIOLOGY

For many years a wide range of diagnostic and therapeutic procedures have been performed by fluoroscopic-aided catheter or device insertion. Currently, ultrasound, X-ray CT, and MRI are used in addition to fluoroscopy to guide the placement of probes with minimal disruption of tissue. The procedures include drainage of fluid from the pericardium, lungs, and abdomen; minimally invasive neurosurgical treatment of arteriovenous malformation of cerebral vessels; treatment of vertebral disk pathology; guided placement of radiation sources; and image controlled freezing or hyperthermia treatment of cancer. The percutaneous approach to surgical treatment depends on contemporary advances in 3-D imaging methodologies and new methods of visualization including virtual reality. Three technological advances that have enabled interventional radiology to replace many surgical methods include the 3-D capabilities of MRI, microfabrication methods for developing miniature surgical tools, and image manipulation and visualization methods.

DIAGNOSTIC RADIOLOGICAL IMAGING

Below the applications of the main methods of diagnostic imaging in human health care are presented under the categories of the body most commonly studied: brain, chest and lung, heart, abdomen, liver, kidneys, female reproductive organs, breast, prostate, and the skeletal system. Some illustrative images are presented as catalogued by Fig. 1. Medical background material and patient-based radiological procedures are found in (9).

BRAIN

Two of the most widely used imaging modalities in the study of the brain, cranial nerves, and spine are X-ray CT and MRI. As X-ray CT is well suited to imaging of bone, calcifications, and hemorrhage, it is still a mainstay of imaging in the emergency room particularly in the evaluation of head and face trauma and in suspected subarachnoid hemorrhage of the brain. With the advent of X-ray CT and MRI, the uses of plain film X rays and injection of air for demarcating the ventricles (i.e., pneumoencephalography) have disappeared. Though ultrasound study of the infant brain is possible because of less attenuation from the infant's underdeveloped skull bone, even applications of ultrasound have been supplanted by X-ray CT and MRI in infants.

Cerebrovascular Diseases (Hemorrhage and Stroke)

A major application of X-ray CT in the emergency room is the evaluation of subarachnoid hemorrhage which is associated with trauma to the head but also occurs spontaneously. Of the spontaneous types 75% occur from the rupture of an arterial aneurysm and 25% occur due to leakage from an arteriovenous malformation. X-ray CT is the diagnostic mode which gives an increased signal from blood in the cerebral spinal fluid spaces. Intracerebral hemorrhage which can occur in hypertension is also best evaluated by X-ray CT which has well-known temporal changes in signal intensity with time after the episode.

Stroke is the result of a disruption of the nutrient blood flow to part of the brain and is a major cause of brain malfunction, particularly in the elderly. A transient stroke known as the transient ischemic attack lasts for 24 h or less, the stroke in evolution causes a progressive neurological defect, and the completed stroke is one in which the neurological defect appears fixed with no or very slow return to some function. MRI if available is the procedure of choice at the onset of symptoms using diffusion-weighted imaging methods. Later due to the cytogenic and then extracellular edema MRI and even X-ray CT can pinpoint the tissues involved. Frequently, the usual MRI study will not reveal the stroke territory until 8 h after the event but the pathology can be detected by diffusion weighted imaging within 15 min of the event. Use of fast imaging methods such as echo-planar MRI will, with a MRI contrast agent, show decrease in regional blood flow.

PET and SPECT techniques can in principle detect a stoppage in flow to regions of the brain at the time of the event because these techniques measure tissue blood flow directly by following the distribution of a flow tracer. The lack of day and night availability of a flow tracer for PET has limited its application to stroke. As PET and SPECT have a major importance in determination of vascular reactivity of compromised regions of the brain they are useful in the staging of patient treatment after the acute phase.

Brain Angiography

The use of contrast X-ray studies in evaluation of the brain vascular system (i.e., cerebral angiography) has to some extent been replaced by magnetic resonance angiography (MRA) though digital subtraction angiography still provides higher resolution images of the vascular tree when very high resolution is diagnostically important. MRA need not require any contrast medium injection as the method uses intrinsic properties of magnetic resonance of moving protons to attain contrast between flowing blood and stationary protons. The phase-sensitive technique uses a bipolar flow encoding gradient to cause a phase shift for a moving proton but a zero phase shift or canceled phase shift for a stationary spins. By reversing the polarity of the flow encoding gradient on alternate acquisitions and subtracting the data from these acquisitions the movement of the protons provides the signal. The time-of-flight method relies on magnetization of spins flowing into an excited volume wherein the stationary spins have been saturated; thus the unsaturated flowing blood will have a detectably higher signal compared with the surrounding previously saturated parenchyma. In addition, recently developed intravascular contrast agents such as a gadolinium–albumin complex have been used with MRI to improve definition of the cerebral vascular system.

Brain Tumors

The prevalence of primary brain tumors in the population is lower than most tumors and other diseases (about 2% of autopsies) yet the importance in diagnosis is vital to health care decisions particularly for metastatic tumors, which constitute 20% of brain tumor diagnoses. The majority of primary tumors are glioblastoma multiforme (25%) and the prognosis for these tumors is poor; however, therapy guided by presurgical and postsurgical MRI does aid in prolonging life with good quality for a few years. The prognosis for meningioma, pituitary adenoma, and acoustic neuroma, which together constitute 32% of brain tumors is very good if detected early, and both MRI and CT have played a major role in the presurgical planning for treatment. Tumors are usually hyperintense on T_2 weighted MRI with a large region of vasogenic edema surrounding the main tumor site (Fig. 9). Though MRI studies provide a wealth of data in brain tumor detection, X-ray CT can in some cases (e.g., meningioma) be as valuable. MRI sequences designed to show blood volume have been useful in defining tumor locations and response to therapy.

PET and SPECT have played a major role in the postsurgical followup of treated tumors. PET imaging following glioblastoma surgery for example can distinguish recurrent tumor from radiation necrosis (Fig. 9); however, recently use of magnetic resonance spectroscopy (MRS) has shown that in areas of recurrent tumor there is an elevated choline signal representative of an increase in one or more of the choline-containing compounds in a tumor.

Brain Neurodegeneration (Alzheimer's Disease and Multiple Sclerosis)

The most common form of neurodegeneration is Alzheimer's disease. As this disease is associated with the atrophy of the hippocampus and the parietal lobe during the early course of the disease, X-ray CT and now more recently MRI have been used to demonstrate the extent of loss of brain mass. Unfortunately, the atrophy of Alzheimer's disease is not dissimilar to that found in normal aging as shown in Fig. 10. PET patterns of a decrease in the parietal lobe glucose metabolism are very characteristic of Alzheimer's disease as is a decrease in blood flow as revealed by either PET or SPECT. The quantification of changes in glucose metabolism do correlate with the progression of the disease and can be used to monitor any efficacy of proposed therapies.

Huntington's and Parkinson's diseases are generally detected by neurological examination but in these two diseases of neurodegeneration of parts of the brain, the X-ray CT and MRI patterns usually appear normal. However, the metabolic data of PET give specific and diagnostic patterns of decreases of glucose metabolism of the caudate nucleus in Huntington's patients and decrease in the dopamine neurochemical system in the central gray matter of Parkinson's patients.

Demyelinating Disorders (Multiple Sclerosis)

MRI is the method of choice in the diagnosis of multiple sclerosis which appears as diffuse lesions of the white matter in the brain of the middle-aged adult. The areas of increased water content are associated with demyelination in regions usually surrounding the ventricles but lesions are found also in the spinal cord and optic nerve. The other demyelinating diseases such as the congenital leukodystrophies have the common characteristic of increased water content of regions of the cerebral white matter.

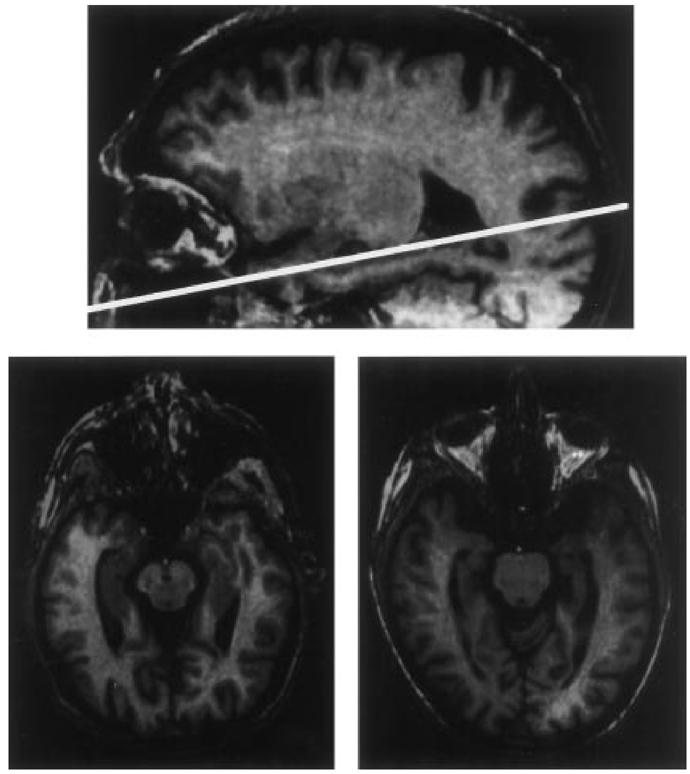

Figure 10. MRI using the 3-D method of gradient recall shows brain atrophy during normal aging of an 86-year-old athlete (lower left) compared with that of a 77-year-old patient with Alzheimer's disease (lower right). The atrophied areas look like two seahorses facing each other on either side of the central brain stem. These seahorselike structures are the hippocampi and are responsible for some memory functions.

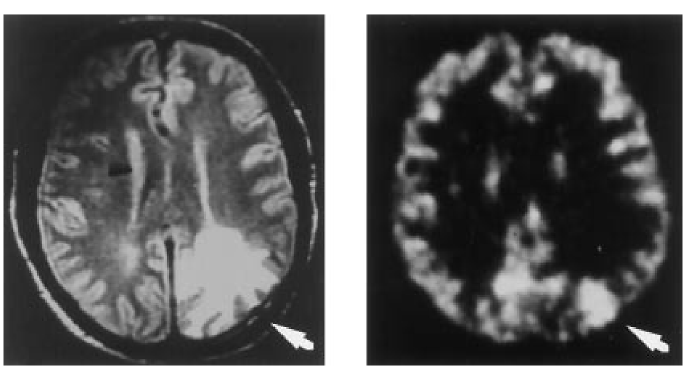

Figure 9. Comparison between MRI spin echo and PET glucose metabolism of a brain tumor. MRI shows increased water and longer T_2 relaxation in and around (edema) the tumor. PET shows increase in glucose metabolism typical of brain tumors. Detection of probable islands of tumors outside the bright spot (arrow) depends on the resolution of the PET scanner.

CHEST (LUNG) RADIOLOGY

The major uses of radiological imaging methods has been in the diagnosis of diseases of the chest or thorax. The major conditions for which radiologic imaging is essential is detection and evaluation of pneumonia (bacterial, fungal or viral), cancer, pulmonary embolism, and chest trauma.

Pneumonia (infective consolidation of the lung) is detected as increased density by the standard X-ray radiograph but the specific diagnosis is not usually made (e.g., 30% to 50% of pneumonias have no causative diagnosis). The most commonly identified organism is *Strep. pneumoniae* (30%) followed by *Hemophilius influenzae, Legionella, Chlamydia,* and *Mycoplasma pneumonias.* Viral pneumonias are uncommon in adults but do predispose to bacterial pneumonias. The standard radiograph usually shows blotchy densities in localized areas sometimes involving both lungs.

Tuberculosis is a bacterial infection with an insignificant incidence until the early 1990s when an increase in incidence occurred related to HIV infections. Densities around the central thorax (i.e., paratracheal and tracheobronchial adenopathy), effusions and patchy and multifocal opacities in the apicoposterior segment of an upper lobe or the apical segment of a lower lobe are common X-ray patterns in tuberculosis.

Lung Cancer

Lung cancer is usually classified into squamous cell carcinoma, adenocarcinoma, and undifferentiated carcinomas which are further divided into small (oat)-cell and large-cell types. Squamous cell carcinoma and adenocarcinoma are found most often. The peak incidence age group is 50 to 60 years old. Once a tumor is suspected, three modalities of imaging are brought to bear: X-ray CT, MRI, and PET (or SPECT). The plain X ray does show patterns which help distinguish bronchioloalveolar carcinoma from the other cell types, and the pattern of size, localization, and numbers of opacities can dictate treatment. Most patients still require an invasive procedure to distinguish a benign from a malignant lesion. Bronchoscopy, percutaneous needle biopsy, thoroscopy, and open lung biopsy have associated risks and do not always provide a definitive answer.

A solitary pulmonary mass or nodule is the single most common presenting sign of bronchial cancer in 40% to 60% of lung cancers. But the majority of diagnosed solitary nodules are not malignant and even the malignant solitary nodules less than 20 mm in diameter can be successfully removed with a 5-year survival of 50%. X-ray CT, MRI, and PET can assist in a major way in staging these patients as these modalities allow evaluation of whether there is disease in the mediastinum in which case surgical resection would not be done as there is extended disease.

Unfortunately most lesions remain undiagnosed and patients usually proceed to biopsy or surgery, which frequently reveals benign processes. In a recent study of radiographically indeterminate thoracoscopically resected solitary pulmonary nodules, 52% were benign (10). Thus, indeterminate lesions remain a dilemma with significant cost and morbidity. FDG PET imaging of thoracic neoplasms has been successful in distinguishing benign from malignant focal pulmonary abnormalities (11), in staging treatment for known malignancies, and in following patients after treatment for neoplasm (Fig. 11).

Once the diagnosis of malignancy has been established, radiographic staging is usually performed using various modalities such as radionuclide bone scanning thoracic X-ray CT and, if available, ^{18}FDG PET. The overall sensitivity and specificity of X-ray CT in detecting intrathoracic lymph node metastases in most series is only about 60%. FDG PET appears to be more sensitive although less specific for malignancy. Surgically proven metastases to hilar and mediastinal lymph nodes as small as 5 mm in diameter have demonstrated increased FDG uptake. After radiotherapy, residual abnormalities noted on chest radiographs can be differentiated as recurrent neoplasm or fibrosis using PET scanning (12).

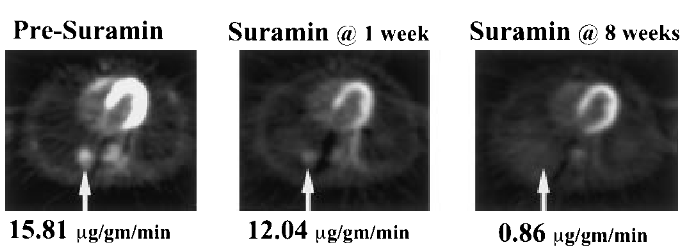

Figure 11. Metabolic response of metastatic prostate cancer to Suramin therapy measured by ^{18}F-fluorodeoxyglucose (^{18}FDG) positron emission tomography (PET). Note also the normal uptake of ^{18}FDG in the left heart muscle whose brightness depends on the nutritional status of the patient (courtesy of C. Hoh, UCLA).

Pulmonary Embolism

Blood clots in the lung circulation represent one of the most serious threats to life in both seriously ill patients, healthy patients in the postsurgical period, and in healthy patients (e.g., travelers in sedentary positions, leg fracture and sprained ankle cases in adults and youths). Postmortem studies have shown that up to 65% of hospitalized patients have emboli lodged in their pulmonary arteries (13) though only 1% have the clinical diagnosis. No single diagnostic test can be regarded as completely reliable in confirming or excluding the diagnosis of pulmonary embolism. In 90% of the cases blood clots arise from thrombosis of the deep veins in the legs. Blood stagnation is the major predisposing cause with only 15% or less of the pulmonary embolism patients having some blood clotting disorder.

Radiological imaging techniques are used in to detect deep vein thrombosis and also to detect the existence of pulmonary embolism by direct radiographic examination of the lungs. Actual detection efforts commence when a patient has some signs of leg thrombosis (e.g., leg pain, swelling). It is important to verify if deep vein thrombosis exists as half of these patients may have had silent pulmonary embolism and a diagnosis leading to therapy (i.e., anticoagulation) is imperative. A second situation is the patient who presents symptoms of pulmonary embolism (e.g., coughing up blood). The deep veins of the legs and possibly pelvis are involved and thrombosis can be detected by injection of X-ray contrast material or a radioactive tracer into the peripheral veins (e.g., foot) and subsequent X ray or radionuclide imaging can detect blockage. But these techniques are imperfect as there are problems in venous access, incomplete filling, and discomfort to the patient. Indeed the patient can have thrombosis induced by the procedure. Of all the methods explored, magnetic resonance angiography seems now to have the potential for detection of deep vein thrombosis (14). Spiral X-ray CT has shown a 90% sensitivity and similar specificity for detection of pulmonary emboli relative to the gold standard of pulmonary angiography (15). More clots are detected with spiral X-ray CT that with pulmonary angiography. Though now considered to be a potential solution to the accurate, noninvasive diagnosis of pulmonary embolism, spiral X-ray CT shows great variability in detecting subsegmental emboli which have a frequency of 6%. This limitation is shared with the gold standard, however.

BREAST CANCER

The incidence of breast cancer has been rising at 3% per year over the last 13 years to a prevalence level of about 0.1% of women in the United States. Since the mid-1980s when X-ray mammography became a readily available screening procedure, 44% of adult American women have had at least one procedure. The mortality rate of breast tumors remains high,

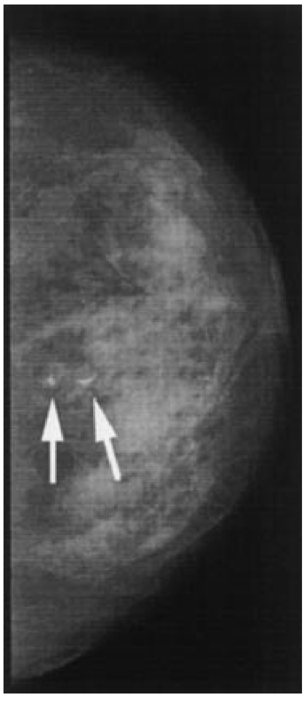

Figure 12. High resolution digitized mammogram which shows microcalcification which could represent breast tumor but confirmation requires a biopsy (courtesy of D. Gur, University of Pittsburgh).

however, at a rate of 25 per 100,000 per year. There are approximately 11,000 dedicated mammography units in the United States. The consensus is that better methods of verification of suspicious lesions detected on X-ray mammography are needed (only 1 in 4 are biopsy positive). In addition, a method is needed to evaluate (screen) patients with radiographically dense breasts. Even the most advanced methods of digital image processing of high resolution mammograms fail to give specific diagnosis in a large fraction of cases (Fig. 12).

Early breast cancers are often identified by planar X-ray mammography. The cost of this examination is low, the spatial resolution high (<100 μm). X-ray mammography is an effective screening technique for detection of cancerous growth in early stages. However, the complexity and heterogeneity of tissue within normal breasts makes unambiguous identification of malignant tumors difficult, as benign tumors and other breast structures can be similar in appearance to cancerous lesions. As a result, a large fraction (50% to 75%) of the suspicious structures identified in mammograms are noncancerous (16) and, thus, further diagnosis is necessary before determining that the patient should be treated for cancer.

This further diagnosis is often obtained by biopsy. The biopsy can determine whether the structure is cancerous, and if so, can also determine the type of cancer and so suggest a course of treatment. The biopsy is time consuming for the physician, often uncomfortable for the patient, can increase the patient's radiation exposure and, unless done by a cytopathologist at the bedside, takes several days before the results of a full assay for tumor type are available.

Should the tumor prove to be cancerous, it is desirable to know before performing surgery whether the cancer has spread to the axillary nodes, as this affects the treatment selection and prognosis (60% to 90% of patients without nodal involvement have no further breast cancers detected in their lifetimes) (16). Nodal involvement is difficult to determine before surgery from an X-ray CT or MRI scan. Nodes can be enlarged for a variety of benign reasons and small tumors difficult to observe by contemporary radiologic imaging methods.

Contrast enhanced MRI has demonstrated a high sensitivity to detection of small (<1 cm) lesions in the breast; however, the specificity is less than 40%. The specificity improves slightly when dynamic techniques are used to measure the rate of contrast agent uptake during the initial minutes after contrast injection (17), but this specificity increase comes at the expense of spatial resolution or full imaging coverage of the breast. The axillary nodes are poorly evaluated with MRI mainly because of the inability to separate involved and uninvolved nodes based on contrast enhancement, as contrast enhancement occurs for both normal and pathological nodes.

Doppler-ultrasound using color to encode velocity or blood volume (power) is another method of evaluating X-ray mammographically detected suspicious lesions before biopsy (18). This method is noninvasive and inexpensive, but it requires a skilled operator and is not envisioned as a screening method. Doppler-ultrasound imaging has been successful in showing which of the suspicious lesions are cancerous and has value in determining lymph node involvement (19) in preliminary detection studies, particularly in those with contrast agents (20).

Positron emission tomography (PET) and the tracer F-18-fluorodeoxyglucose (^{18}FDG) can provide excellent sensitivity for malignant breast tumors and axillary node involvement. Because of the expense and limited availability of PET, single photon methods (SPECT, Gamma camera imaging, scintimammography) can play a major role in the differential diagnosis of suspicious X-ray mammography lesions. The specificity of the radiopharmaceutical ^{99m}Tc-sestamibi for axillary node involvement with breast cancer ranges from 42% to 88%. This specificity, though better than X-ray mammography, could be increased by an improved detector system. It is believed that the 8% to 20% of tumors that are not revealed by ^{99m}Tc-sestamibi and those below 1.5 cm in diameter could be detected if the limitations of contemporary gamma cameras are overcome.

Contemporary scintimammography and SPECT studies use large field of view gamma cameras which use a scintillator block coupled to a bulky array of photomultiplier tubes. By nature of their large size, these instruments are inadequate in most clinical situations because imaging of small organs such as the breast is usually awkward due to the fact that close access to the breast and axillae is prevented by the camera housing imaging system (Fig. 13). Solid state cameras have the potential to overcome these limitations.

HEART

There are multiple methods used for examination of the human heart: ultrasound, X-ray coronary angiography, magnetic resonance imaging (MRI), magnetic resonance angiography (MRA), and nuclear medicine imaging methods (PET and SPECT). Ultrasound is used in the cardiologist's office for

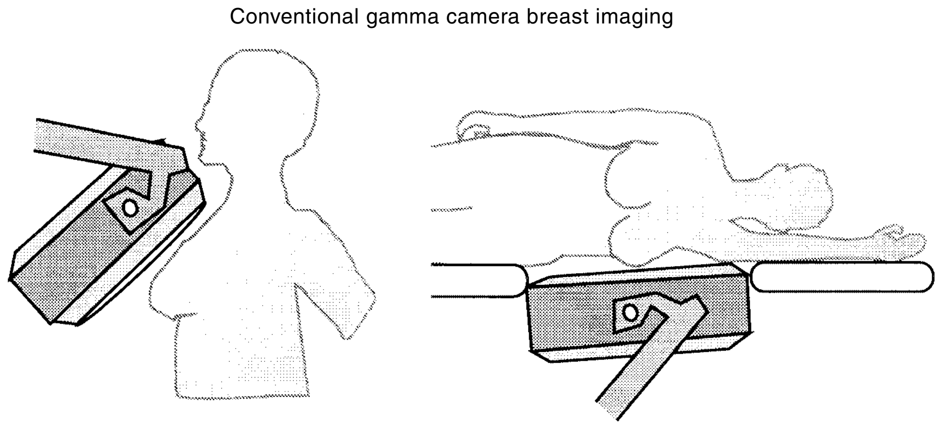

Figure 13. A major problem in breast imaging with conventional gamma cameras is to get close to the probable cancer site. Compact solid state imaging systems currently being designed for the breast can overcome this problem.

evaluation of valvular function using the M-mode method wherein motion of the valves is recorded as reflected signal distance versus the temporal sequence of the cardiac cycles. Using the 2-D imaging mode, the surface of much of the heart muscle can be imaged on-line, thus abnormalities in the synchronous motion of the contracting and expanding heart can be visualized by the cardiologist and changes of the heart muscle thickening during infusion of mild pharmacological stress can give evidence of the health of the heart. Ultrasound contrast agents using microbubbles have been introduced recently to aid in imaging the heart chambers and flow dynamics.

Magnetic resonance imaging can also image the motion of the walls of the heart during each heart beat and though currently more cumbersome to operate, MRI has more complete coverage of the heart than ultrasound particularly on obese patients or patients with large breasts. MRI can also show fine detail of wall motion by specifically showing the muscle motion. A grid of saturated image pixels is placed over the heart slice using a saturating RF pulse sequence. The heart is then imaged during the cardiac cycle and the saturated pixels move with the pixel elements thus allowing determination of muscle motion and calculation of strain. Alternatively, the motion of each pixel can be deducted by phase changes associated with motion and the trajectories of muscle displacements.

Nuclear medicine methods are employed in the evaluation of ischemic heart disease. The most common test is evaluation of the difference in perfusion between rest and stress induced by treadmill exercise or a pharmacological agent. In the absence of flow from an obstructed coronary artery, no tracer will reach part of the heart muscle fed by that artery and a hole will appear on the image. Frequently, when there is some but diminished flow to part of the heart, this difference between normal and low flow can be amplified by stressing the heart which increases the flow to normal tissue by as much as fourfold without any significant increase in flow to the compromised tissue. The difference between rest images and stress images is used to diagnose viable from infarcted tissue.

As emission methods do allow specific chemical and metabolic processes to be detected, PET has been used to show glucose uptake (see heart uptake in Fig. 11), fatty acid metabolism, and neurochemical status of the heart. It has been discovered that the viable but jeopardized (low coronary flow) regions of the heart accumulate an analogue of glucose labeled with ^{18}F and this fact has been used to show that patients with a seeming absence of flow by perfusion methods but an accumulation of FDG do have some viable tissue and are candidates for revascularization surgery.

Coronary Angiography

The major use of X-ray imaging of the heart other than the routine chest X ray is coronary catheterization performed for the detection of coronary atherosclerosis. The procedure involves inserting a catheter in the femoral artery of the groin and feeding this catheter into the opening to the left and right coronary arteries which are at the aorta near the base of the heart. Contrast material having a high concentration of iodine is injected selectively into each coronary artery. Separate catheters are usually used for each coronary and the procedure is carried out by the cardiologist or radiologist in a hospital setting. This procedure, though considered the gold standard for definitive diagnosis of coronary athersosclerosis, is uncomfortable and costly, thus alternative methods for evaluation of the heart have been sought.

MR angiography with or without use of MR contrast material is used to show the lumen of vessels just as is done with X-ray arteriography but presently with less resolution. In theory it is possible to image the coronary artery down to about 0.5 mm using intravascular contrast material and fast imaging methods and this modality could replace the commonly performed coronary catheterization (Fig. 14).

Coronary Artery Calcification Detection

Calcification of the coronary arteries increases with age in the asymptomatic population, but the quantity of coronary artery calcification is high in patients with clinically symptomatic coronary artery disease. Calcification is detected by intracoronary ultrasound and noninvasively by fast CT or electron beam CT (EBCT) wherein 100 ms duration scan times and EKG gating minimize motion blurring, which have hindered fluoroscopic and conventional CT for detection and quantification of calcium deposits. The fact that 8% of the asymptomatic subjects have calcium quantities above the 75th percentile for age and sex has led to the recommendation that older patients with risk factors (e.g., high cholesterol) for a coronary event have an EBCT (21).

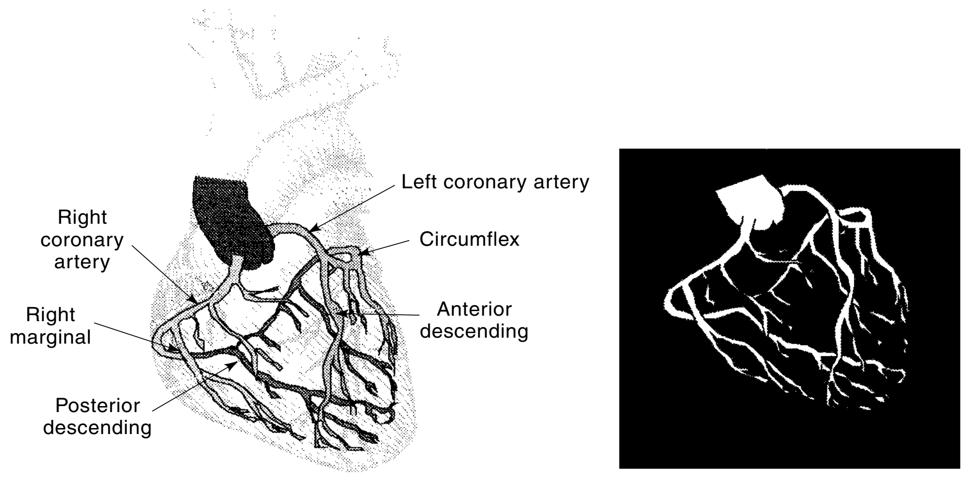

Figure 14. Coronary angiography using invasive catheters is expected to be replaced by noninvasive MRI using spiral imaging methods and intravascular contrast material. This is a cartoon of the coronary arterial tree.

GASTROINTESTINAL

Liver

Two major radiological applications of ultrasound have been detection of primary and secondary cancer of the liver and gallstones in the gallbladder. The principal radiological diagnostic problem in the evaluation of the liver is the detection of cancer metastases from cancers elsewhere in the body and the differentiation of solid tumor masses from cysts, abscesses, and hemangiomas. Liver imaging is also valuable in evaluation of cirrhosis and fatty infiltration. X-ray CT with contrast agents, ultrasound, radionuclide methods, MRI, and most recently spiral X-ray CT have been compared in their accuracy to detect and differentiate liver lesions (22). The accuracy of US and CT is generally believed to be about 60% to 80%.

A major problem of liver imaging in the past has been blurring and artifacts from normal liver motion during the tomographic scan. Motion, until recently, has rendered MRI less valuable than ultrasound or X-ray CT. But since 1994 methods of compensation for motion and faster imaging strategies of MRI and spiral X-ray CT have resulted in significant improvement in diagnoses. X-ray CT is the most widely used cross-sectional method for liver tumor evaluation in the United States. However, with the introduction of different MRI contrast agents which have specificity for normal parenchymal Kupfer cells, extracellular space or blood pool, the diagnostic potential of MRI might compete with spiral X-ray CT and possibly avoid needle biopsy frequently required to make the diagnosis of liver masses. MRI is the best technique for evaluating fatty infiltration and both MRI and ultrasound are effective in evaluating liver vasculature.

Colorectal Tumors

Colorectal tumors are usually suspected from symptoms of pain and bleeding with confirmation by conventional barium enema and colonoscopy. Since 1990, spiral X-ray CT (see above) has been utilized for the study of the abdomen and pelvis because the rapid coverage avoids motion artifacts from respiratory-based organ motion. Spiral X-ray CT data from the air-filled colon has been used effectively and is the basis for virtual colonoscopy. A major diagnostic problem is the evaluation of tumor therapy. PET was found to be superior to pelvis X-ray CT in detecting local disease recurrence (23). The accuracy for local disease recurrence was 95% for PET and 65% for pelvis CT. No significant difference was found for the accuracy in detecting lesions in the liver, 98% for PET and 93% for CT or US. PET whole body scanning detects dissemination of colorectal tumors (24).

GENITAL AND URINARY

Fetus and Pregnancy

Ultrasound using either an abdominal probe or a transvaginal probe is used to confirm the presence of intrauterine pregnancy at 4 to 5 weeks of gestation, the heart beat at 6 weeks, and subsequently the normal or abnormal development as well as the gestational age by the length of the embryo/fetus.

Abdominal sonography has a vital role in deciding whether amniocentesis should be performed for genetic purposes and for detection of lung maturity. The electronic control of data from modern ultrasound transducers (Fig. 3) allows three-dimensional data extraction such that the face and other surfaces of the fetus can be visualized in utero (Fig. 15).

Other uses of ultrasound relative to pregnancy are evaluation of causes of infertility, facilitation of embryo transfer, and investigation of causes of abdominal pain and masses, because X-ray methods are not used due to concern of exposing the fetus to ionizing radiation. MRI procedures are not in widespread accepted use at least in the first 2 trimesters though there is no known reason not to take advantage of MRI diagnostic capabilities throughout pregnancy.

Female Reproductive Organ Cancer

Ultrasound of the female pelvis is routinely used to depict the normal pelvic anatomy and to demonstrate both physiological and pathological changes of the ovaries, uterus, and cervix. Whereas ultrasound at 3.5 to 5 MHz provides diagnostic information of clinically suspected disease, X-ray CT and MRI are used to provide accurate localization for both biopsy and radiotherapy.

Carcinoma of the uterine cervix is the second most common malignancy in women and accounts for two-thirds of ma-

Figure 15. Three-dimensional ultrasound image of the face and hands of a normal fetus in the mother's uterus (courtesy of Aloka Co. Ltd.).

lignant tumors found in the female genital tract. Neither ultrasound nor X-ray CT are clinically useful in the diagnosis of early disease, but X-ray CT can show local spread in more advanced disease. MRI is now established as a highly accurate method of demonstrating invasive cervical carcinoma but in early disease MRI underestimates superficial cervical carcinoma. These modalities are also of limited effectiveness in detection of carcinoma of the uterus which is one-third as common as cervical carcinoma. X-ray CT for uterine cancer requires use of intravenous contrast which enters the normal myometrium better than into the cancer. A common benign but clinically important condition of the uterus is fibroids which are usually accurately detected by ultrasound.

Both ultrasound and X-ray CT are used in the definition of ovarian tumors and cysts but the differentiation is frequently difficult. The accuracy of MRI in distinguishing benign from malignant ovarian cancers remains controversial. Overall imaging techniques currently have a limited supportive role in the initial assessment of ovarian cancer but MRI appears to be superior in depicting local tumor infiltration of the bladder, pelvic fat, and other tissues including metastases to the liver and local invasion of the myometrium. Although MRI is superior to X-ray CT, X-ray CT is currently preferred for the assessment of the entire abdominoperitoneal cavity as it is more widely available, less expensive, and is a method with which there is a vast experience.

Kidney

The major diseases for which radiological procedures are needed include, kidney injury, kidney artery stenosis (e.g., atherosclerosis), kidney failure, kidney carcinoma, and kidney transplant rejection. X-ray CT, ultrasound, radionuclide procedures, and MRI all have a role in the diagnosis of kidney disease. X-ray CT is the procedure of choice in evaluation of the patient with suspected kidney trauma. Use of spiral X-ray CT with breadth holding and contrast agents provides a comprehensive evaluation for many situations; however, equivalent and in some cases supplemental information can be gleaned from use of fast MRI methods with injected contrast material (e.g., Gd-DTPA) as shown by the comparison in Fig. 16. Ultrasound methods provide a convenient approach to determination of dilation of the collection system in order to determine the presence of obstruction which can be caused by obstruction of an ureter or even benign prostatic hypertrophy.

Prostate

The two major diseases of the prostate gland are benign prostatic hypertrophy and prostate cancer. Prostatitis is an acute or chronic bacterial infection diagnosed and treated medically. Prostate cancer is the second commonest cause of cancer death in American men over age 55. It is the commonest human cancer found at autopsy in 30% of men at age 50 and in 90% at age 90 but usually as a latent disease. The best techniques for early diagnosis are measurement of prostatic serum antigen (PSA) and the rectal exam. The radiological procedures are transrectal ultrasound (TRUS) and transrectal MRI. Though neither technique can definitively separate prostatitis from carcinoma in all cases, both techniques can help define the likelihood of cancer and TRUS as well as X-ray CT are used to guide biopsy needles to confirm cancer and metastases. Both techniques help define whether the cancer has invaded the capsule or tissues outside the prostate and therefore aid in the therapeutic choices. When cancers are confined to the prostate gland they are curable by surgical removal of the prostate gland. X-ray CT is not now used for routine tumor staging but is useful in advanced cancer when lymph nodes are enlarged.

PET and SPECT are not useful in defining the primary disease because radionuclide accumulation in the bladder interferes with imaging the adjacent prostate. The prostate tumor metastases have low avidity for static accumulation of fluorodeoxyglucose (FDG) in bone but soft tissue metastases are detected by PET (Fig. 11). Recently, MRS (magnetic resonance spectroscopy) superposed on MRI has been effective in detection of prostatic tumors and in evaluation of therapy us-

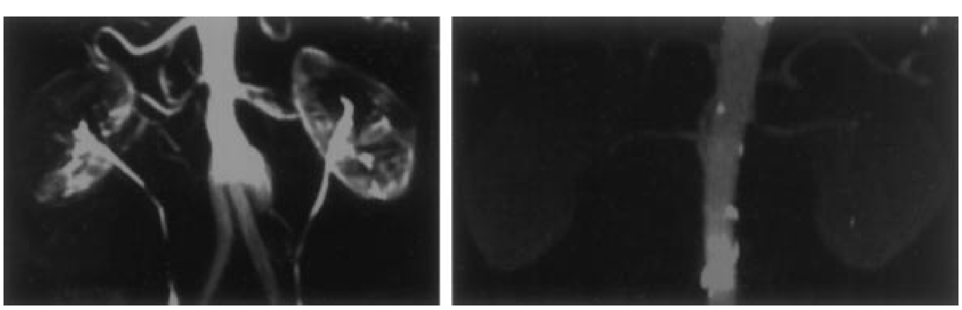

Figure 16. Fast MRI with contrast material (left—courtesy of GE Medical Systems) reveals major vessels as well as kidney function through visualization of the ureter because the contrast material is excreted into the ureters by the kidney. X-ray CT (right—courtesy of Siemens Medical Systems) using contrast material shows vessels and the presence of severe atherosclerosis revealed by multiple large calcium deposits in the aorta.

ing an image of the ratio of choline containing compounds to citrate obtained from spatial maps of spectral information or chemical shift imaging. The normal prostate shows a high concentration of citrate on proton MRS and tumors have a relatively high signal from the trimethyl groups of choline-containing compounds.

SKELETAL SYSTEM

Joint Disease

The three main categories of joint disease are injury, rheumatoid arthritis, and osteoarthritis. The important tissues of the joint are the synovial membrane, which is like a sleeve around the joint; the cartilage material on the surfaces of the articulating bones, which provides a low coefficient of friction surface allowing smooth joint motion; and the ligaments and tendons, which attach the articulating surfaces or are attached to these surfaces.

Athletic injuries to shoulders and knees are common injuries which require diagnostic methods of X-ray CT and MRI. MRI has provided a major advance in the diagnostic imaging of the shoulder (rotator cuff) and knee (meniscus, cartilage) injuries (Fig. 17). Meniscal MRI, however, has a unique role. In many circumstances it substitutes for other techniques that are either less accurate (physical examination); largely operator dependent, mildly invasive and expensive (i.e., arthrography and diagnostic arthroscopy). MRI of the knee menisci is one of the most efficient uses of this technology. Although MRI certainly has a role in evaluating muscle, tendon, and ligament pathology in the knee, clinical assessment determines therapy.

Rheumatoid arthritis is a systemic disease and at the joint level major pathophysiological mechanisms include immune, inflammatory, and healing or remodeling reactions. This disease starts as an inflammatory reaction of the synovium from an unknown cause. This reaction attracts white blood cells with a resulting swelling, edema, and soft tissue laxivity, thus weakening the joint and causing dysjunction between opposing bones. The nutrient supply to the cartilage is from nonvascular diffusion into and out of the synovium; thus, processes which influence the function of the synovium will inevitably affect functioning of cartilage which depends on a balance between collagen, protein polysaccharide matrix, water, and ions for its health.

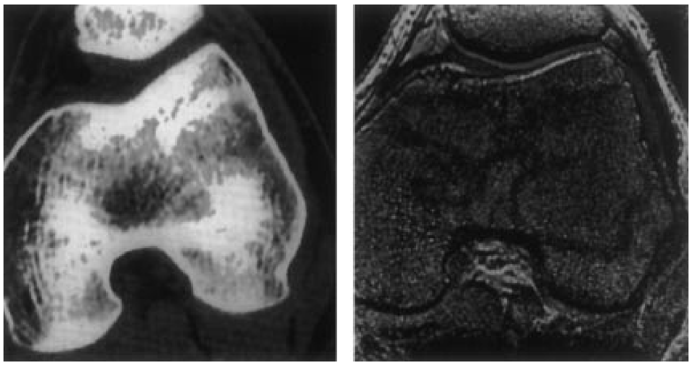

Figure 17. Different types of information provided by X-ray CT and high resolution MRI of the human knee (right—courtesy of S. Majumdar, University of California, San Francisco). The difference in magnetic susceptibility between trabeculae of bone and marrow allows high resolution and high contrast imaging.

Uncontrolled inflammatory responses of the white cells break down collagen and components of the cartilage with eventual destruction of the cartilage, a narrowing of the joint space and destruction of the adjacent surfaces of the bone of the joint. There also occurs a loss of bone early in the disease due to the inflammatory reaction which causes increased local destruction of the bone. The pattern of rheumatoid arthritis is also associated with some general disorders such as systemic lupus erythematosis, ankylosing spondylitis, scleroderma, and juvenile chronic polyarthritis but there is a high prevalence of rheumatoid arthritis of the extremities with no known etiology.

The radiological pattern of rheumatoid arthritis is that of progressive changes in the joint tissue symmetry, bone alignments, and patterns of swelling which can be chronic or intermittent. Osteopenia (local regions of loss of bone mineralization) inevitably occur in spite of the treatment. These patterns are readily observed by plane X-ray examination of the hands and other joint spaces. MRI now can give exquisite details of synovium and cartilage changes (Fig. 17) particularly using sequences such as magnetization transfer.

Osterarthritis is the most common joint disease and is characterized by noninflammatory cartilage loss accompanied by new bone formation. Joint trauma and joints undergoing repeated stress [knees and ankles of athletes (Fig. 17) and laborers] are probably the major causes of what is known as secondary osteoarthritis. The primary osteoarthritis currently of unknown etiology is believed to be the result of an intrinsic abnormality of cartilage leading to its degeneration. Both types have the radiological pattern of joint space narrowing and sclerosis of the opposing surfaces of subchondral bone. Deviations and subluxations between articulating bones develop slowly particularly in the fingers and knees. The abnormal bone growth in the fingers is often noted in the elderly as joint prominences known as Heberden's nodes. The radiological pattern of narrowed joint spaces is easily visualized by the standard X-ray, but MRI can give much more detail of the pathology. Figure 18 shows a comparison of spiral X-ray CT and high resolution MRI of the knee, tibia and patella.

Vertebral Spine Diseases

Degenerative disk disease is the most common pathology of the vertebrae and may occur anywhere in the spine but is most dominant in the lower cervical and lower lumbar spine. It is characterized by disk-space narrowing, sclerosis of the vertebral body endplates, generation of osteophytes (bone spurs). The basis for much of lumbar spine disease is from the disk cartilage degeneration due to abnormal physical stress-related biomechanical factors but also narrowing of the spinal column (spinal stenosis) by abnormal bone growth during aging plays an important role in progressive low back spinal cord symptoms. Abnormally high or sustained loading on the human disk cartilage results in water absorption from the nucleus pulposa by adjacent vertebrae, osmotic pressure change in the cartilage, stress on the collagen fibers of the disk annulus, bulging of the disk, and subsequent encroachment of disk material on the nerve roots. Congenital or acquired narrowing of the spinal canal (spinal stenosis) through abnor-

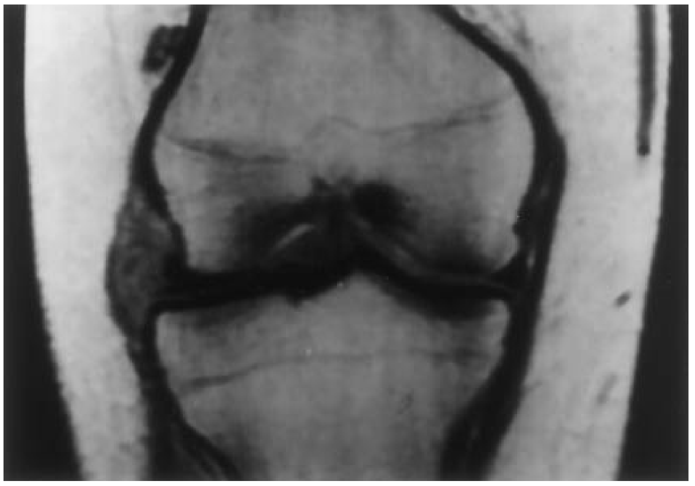

Figure 18. MRI of joints can demonstrate defects in cartilage, ligaments, and bone with greater specificity than possible by other methods including arthroscopy. This image shows a lateral meniscus tear and cyst of the knee (courtesy of D. Rubin, University of Pittsburgh).

mal bone growth is frequently associated with disk disease. Spurs of the bony process of the joints of Luschka in the cervical spine result frequently in neurological compressive symptoms. Comprehensive evaluation of debilitating symptoms of spinal column and nerve root compression is now provided by MRI examination of the cervical and lumbar regions (Fig. 19).

Bone Tumors

Bone tumors and tumorlike lesions are most commonly detected by conventional radiography. MRI and X-ray CT are used to determine the extent of the tumor. MRI's capability to distinguish general tissue types has been valuable in differentiating benign from malignant tumors. Radionuclide imaging is used to evaluate metastases of nonbone tumors (e.g., lung, prostate, and breast) to bone. For this purpose conventional gamma camera planar imaging (scintigraphy) is one of the most often performed nuclear medicine procedure after injection of ^{99m}Tc-phosphate complex (e.g., pyrophosphate, diphosphate salt). The ^{99m}Tccomplex is readily available at all hospitals with a gamma camera and after injection 50% of these bone seeking radiotracers is deposited in the body skeleton as a technetium–calcium–phosphate complex one hour after injection. Whole body planar images are obtained. The amount of local uptake reflects the metabolic state independent of the amount of bone mineralization. The increase in blood flow accompanying the presence of increased metabolism is the major cause for increased uptake in tumors and areas of rapid bone turnover (e.g., osteoarthritis).

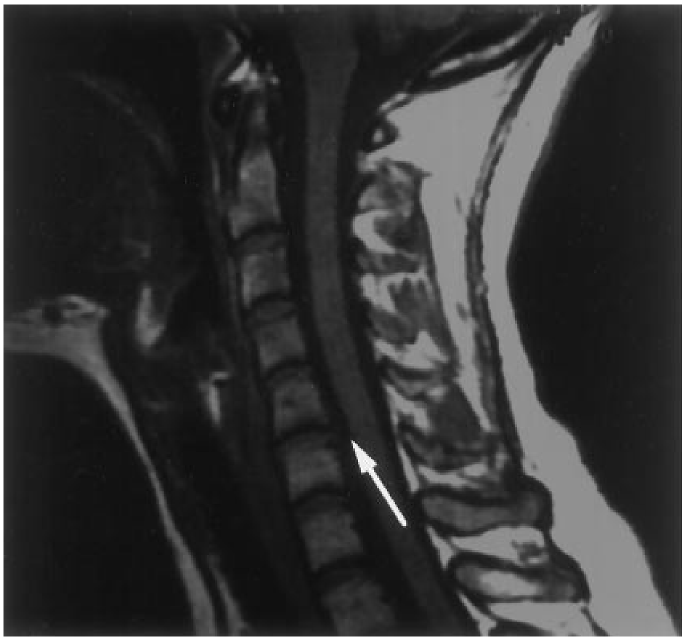

Figure 19. MRI of sagittal view through the cervical spine shows a disk defect which is impinging on the spinal cord. MRI of the spine is also the optimum diagnostic imaging method for low back pain.

Osteoporosis

Osteoporosis is the most common metabolic bone disorder beginning in the fifth or sixth decade in women and the sixth or seventh decade in men. The loss of bone mineral is 3% to 10% per decade. The prevalence of osteoporosis in the aged is high and usually evades routine diagnosis because as much as 60% of bone mineral loss will occur before the osteopenia is detected on conventional X-ray examination. Postmenopausal osteoporosis is identified by a fracture pattern involving vertebral bodies and frequently the wrist (distal radius). Senile osteoporosis presents by fractures involving the hip and vertebrae. There is bone loss of both trabeculae and cortex but in the main the loss is of secondary trabeculae. Fractures in the elderly following minimal trauma as well as back pain frequently lead to diagnostic examination of bone density quantitation using two energy bands of photons either from a dual gamma ray emitting radionuclide such as gadolinium-153 or a single X-ray source operated with filters or different energies to provide two energy bands such that the differential absorption between calcium and the elements of soft tissue can be measured. The bone density is interpreted as a percentage change from a normal or from that expected for a given age. Recent advances in MRI high resolution imaging show promise of providing architectural information of trabecular bone undergoing changes as shown by a comparison between high resolution X-ray CT and high resolution MRI of the knee (Fig. 18).

Vascular System

Radiological methods of imaging the arteries and veins of the body generally have used injection of iodinated contrast material followed by rapid imaging using plane X-ray film or digital subtraction methods. These methods involved inserting catheters in arteries and though precise in diagnostic specificity, they have some morbidity. Yet they remain the major methods for identification of atherosclerosis in brain, carotid, coronary, renal, aorta, and leg arteries. There are three methods of visualizing these arteries using MRI. The phase-sensitive technique uses a bipolar flow encoding gradient to cause a phase shift for a moving proton but a zero phase shift or canceled phase shift for a stationary spin. By reversing the polarity of the flow encoding gradient on alternate acquisitions and subtracting these acquisitions the movement of the protons provides the signal. The time-of flight method relies on magnetization of spins into an excited volume wherein the spins have been saturated thus the unsaturated flowing blood will have a detectably higher signal compared to the surrounding previously saturated parenchyma.

A third method which will replace much of the conventional X-ray angiography uses injected contrast material which unlike previously used MRA contrast material stays in the blood pool (intravascular contrast). This material is gadolinium complexed to albumin which does not diffuse into tissues due to the large molecular size of albumin. The new contrast material overcomes limitations of the past related to temporal changes of contrast material which diffuses through the extracellular space. Image acquisition from moving organs and an imaging time not dependent on the rapidly changing concentration of the injected bolus allows high-resolution angiography. This method has promise to visualize most of the important elements of the arterial blood pool including the coronary arteries down to less than 1 mm before year 2000 (see Fig. 14).

Flow quantitation particularly in the carotid arteries has been provided by Doppler ultrasound techniques which are in widespread use and when combined with ultrasound imaging the method is known as duplex scanning. Doppler images in color denoting direction (red for artery and blue for venous) with intensity related to speed are superposed on the gray level 2-D image which for the carotid shows the vessel and surrounding soft tissues. A new technique known as Power Doppler superposes the intensity of the Doppler signal rather than direction and speed thus this image represents the volume of moving red cells. This technique has been applied with success to a number of problems including detection of malignant lymph nodes from breast cancer and evaluation of kidney disease.

Picture Archiving and Communication System (PACS)

A major component of diagnostic radiology is the digital data-based image storage, transfer, and processing systems embodied in software and hardware of PACS (picture archiving and communications system). PACS, developed many years ago for archiving and digitally transferring conventional radiographs after digitization, has established the methodologies and formats needed for the management of digital data acquired by contemporary radiologic imaging devices (e.g., MRI, PET, SPECT, US) (25). The very high bandwidth data currently being handled by PACS includes cardiac angiography image sequence involving 512×512 images taken at 30 frames per second. For transmission and display, optical fiber-based networks based on asynchronous transfer mode (ATM) are used. Workstations for review of these data can handle a complete or full injection sequence in "loop RAM (random access memory)" using the 512×512 format interpolated to 1024×1024 while displaying at 30 frames per second.

A common standard for image transfer, storage, and retrieval is the DICOM (digital imaging and communications in medicine) standard. Standards for interfacing image data acquired by different modalities (PACS) with radiology information systems (RIS) and hospital information systems (HIS) will allow integration of patient images with the radiologist's interpretation, clinical data, and demographic information for ready access by authorized health-care personnel. These capabilities enable a new dimension in teleconferencing and local workstation-based image processing for 3-D visualization, segmentation, and contrast enhancement. This technology not only enables rapid access to patient information but expedites consultation, education, and research.

ACKNOWLEDGMENTS

This work was supported by the Office of Health and Environmental Research of the U.S. Department of Energy under contract DE-AC03-76SF00098 and National Heart, Lung, and Blood Institute. Dr. Kathleen Brennan assisted in the manuscript.

BIBLIOGRAPHY

1. E. Krestel (ed.), *Imaging Systems for Medical Diagnostics,* Berlin and Munich: Siemens, 1990.
2. J. D. Bronzino (ed.), *The Biomedical Engineering Handbook,* Boca Raton: CRC Press, IEEE Press, 1995.
3. T. F. Budinger et al. (ed.), *Mathematics and Physics of Emerging Biomedical Imaging,* Washington, DC: National Academy Press, 1996.
4. W. A. Kalender et al., Spiral volumetric CT with single-breath-hold technique, continuous transport, and continuous scanner rotation, *Radiol.,* **176** (1): 181–3, 1990.
5. S. A. Feig and M. J. Yaffe, Digital mammography, computer-aided diagnosis, and telemammography, *Radiol. Clinics North Amer.,* **33** (6): 1205–30, 1995.
6. A. Haase et al., FLASH imaging. Rapid NMR imaging using low flip-angle pulses, *J. Magn. Resonance,* **67**: 258, 1996.
7. S. R. Cherry and M. E. Phelps, Positron Emission Tomography: Methods and instrumentation, in M. P. Sandler et al. (eds.), *Diagnostic Nuclear Medicine,* Baltimore: Williams & Wilkins, 1995, pp. 121–138.
8. T. F. Budinger, Single Photon Emission Computed Tomography, in M. P. Sandler et al. (eds.), *Diagnostic Nuclear Medicine,* Baltimore: Williams & Wilkins, 1995, pp. 121–138.
9. J. B. Wyngaarden and L. H. Smith Jr. (eds.), *Textbook of Medicines,* Philadelphia: Saunders, 1988.
10. M. J. Mack et al., Thoracoscopy for the diagnosis of the indeterminate solitary pulmonary nodule, *Ann. Thoracic Surg.,* **56** (4): 825–30, discussion 830–2, 1993.
11. E. F. J. Patz and P. C. Goodman, Positron emission tomography imaging of the thorax, *Radiol. Clinics North Amer.,* **32** (4): 811–23, 1994.
12. E. E. Kim et al., Differentiation of residual or recurrent tumors from post-treatment changes with F-18 FDG PET, *Radiographics,* **12**: 269–279, 1992.
13. D. G. Freiman, J. Suyemoto, and S. Wessler, Frequency of thromboembolism in man, *New England J. Med.,* **272**: 1278–1280, 1965.
14. C. E. Spritzer et al., Detection of deep venous thrombosis by magnetic resonance imaging, *Chest,* **104** (1): 54–60, 1993.
15. M. Remy-Jardin et al., Diagnosis of pulmonary embolism with spiral CT: Comparison with pulmonary angiography and scintigraphy, *Radiol.,* **200** (3): 699–706, 1996.
16. Institute of Medicine (ed.), *Strategies for Managing the Breast Cancer Research Program,* Washington, DC: National Academy of Sciences Institute of Medicine, 1993.
17. S. H. Heywang et al., Dynamische kontrastmittelunteruschungen mit FLASH bei kernspintomographie der mamma, *Digitale Bildiagn,* **8**: 7–13, 1988.

18. R. P. Kedar et al., Automated quantification of color Doppler signals: A preliminary study in breast tumors. *Radiol.,* **197**: 39–43, 1995.
19. C. I. Perre, V. C. M. Koot, and P. de Hooge, Colour Doppler ultrasonography in the diagnosis of axillary lymph node metastases in breast cancer, *The Breast,* **5**: 10–12, 1996.
20. R. P. Kedar et al., Microbubble contrast agent for color Doppler US: Effect on breast masses. Work in progress, *Radiol.,* **3** 679–686, 1996.
21. R. B. Kaufmann et al., Quantity of coronary artery calcium detected by electron beam computed tomography in asymptomatic subjects and angiographically studied patients. *Mayo Clinic Proc.,* **70**: 223–232, 1995.
22. R. E. Larson et al., Hypervascular malignant liver lesions: Comparison of various MR imaging pulse sequences and dynamic CT, *Radiol.,* **192** (2): 393–9, 1994.
23. C. Schiepers et al., Contribution of PET in the diagnosis of recurrent colorectal cancer: Comparison with conventional imaging, *Eur. J. Surg. Oncol.,* **21** (5): 517–522, 1995.
24. G. Beets et al., Clinical value of whole-body positron emission tomography with [18F]fluorodeoxyglucose in recurrent colorectal cancer, *Brit. J. Surg.,* **81** (11): 1666–1670, 1994.
25. H. K. Huang, *PACS: Basic Principles and Applications.* New York: Wiley, 1998.

THOMAS F. BUDINGER
University of California at Berkeley

DIAGNOSTICS, PROGRAM. See PROGRAM DIAGNOSTICS.